NEURAL REGENERATION RESEARCH
Volume 8, Issue 16, June 2013

www.nrronline.org

doi:10.3969/j.issn.1673-5374.2013.16.005 [http://www.nrronline.org; http://www.sjzsyj.org]
Yao XF, Wang MN, Chen XR, Nie SD, Li ZX, Xu XP, Zhang XL, Song ZJ. Diffusion tensor imaging fiber tracking with reliable tracking orientation and flexible step size. Neural Regen Res. 2013;8(16):1481-1490.

Diffusion tensor imaging fiber tracking with reliable tracking orientation and flexible step size☆

Xufeng Yao[1, 2], Manning Wang[2], Xinrong Chen[2], Shengdong Nie[1], Zhexu Li[1], Xiaoping Xu[1], Xuelong Zhang[1], Zhijian Song[2]

1 *Shanghai Medical Instrument College, School of Optical-Electrical and Computer Engineering, University of Shanghai for Science and Technology, Shanghai 200091, China*
2 *Digital Medical Research Center, Shanghai Medical School, Fudan University/The Key Laboratory of MICCAI of Shanghai, Shanghai 200032, China*

Abstract
We propose a method of reliable tracking orientation and flexible step size fiber tracking. A new directional strategy was defined to select one optimal tracking orientation from each directional set, which was based on the single-tensor model and the two-tensor model. The directional set of planar voxels contained three tracking directions: two from the two-tensor model and one from the single-tensor model. The directional set of linear voxels contained only one principal vector. In addition, a flexible step size, rather than fixable step sizes, was implemented to improve the accuracy of fiber tracking. We used two sets of human data to assess the performance of our method; one was from a healthy volunteer and the other from a patient with low-grade glioma. Results verified that our method was superior to the single-tensor Fiber Assignment by Continuous Tracking and the two-tensor eXtended Streamline Tractography for showing detailed images of fiber bundles.

Key Words
neural regeneration; neuroimaging; fiber tracking; two-tensor model; single-tensor model; flexible step size; tracking orientation; fiber bundles; diffusion tensor imaging; grants-supported paper; neuroregeneration

Research Highlights
(1) There is no gold standard to verify brain fiber tracking. There are several diffusion tensor fiber imaging methods including the linear method, probabilistic method, and the energy minimization method. Branching of fiber bundles and high accuracy fiber tracking are important in neuroimaging studies, for which the linear method is extensively used. The multiple-tensor model for solving the problem of branching is also becoming increasingly popular.
(2) We propose a novel linear method that can reveal more real fiber bundles compared with single-tensor Fiber Assignment by Continuous Tracking and two-tensor eXtended Streamline Tractography, and which was consistent with the anatomical structure. Our method used a tracking orientation choice and a flexible step size to ensure the reliability of tracking.
(3) We used human data to compare tracking outcomes of reliable tracking orientation and flexible step size fiber tracking with single-tensor Fiber Assignment by Continuous Tracking and two-tensor eXtended Streamline Tractography in a healthy volunteer and a patient with low-grade glioma.
(4) We qualitatively and quantitatively assessed the advantages and disadvantages of our method, single-tensor Fiber Assignment by Continuous Tracking, and two-tensor eXtended Streamline Tractography.
(5) Our method was superior to the single-tensor Fiber Assignment by Continuous Tracking and the two-tensor eXtended Streamline Tractography for detailed visualization of fiber bundles.

Corresponding author: Xufeng Yao☆, Ph.D., Lecturer, Shanghai Medical Instrument College, School of Optical-Electrical and Computer Engineering, University of Shanghai for Science and Technology, Shanghai 200091, China; Digital Medical Research Center, Shanghai Medical School, Fudan University/ The Key Laboratory of MICCAI of Shanghai, Shanghai 200032, China, yao6636329@hotmail.com. Zhijian Song, Ph.D., Professor, Digital Medical Research Center, Shanghai Medical School, Fudan University/The Key Laboratory of MICCAI of Shanghai, Shanghai 200032, China, zjsong@fudan.edu.cn.

Received: 2013-01-29
Accepted: 2013-04-20
(N20120523006)

INTRODUCTION

Magnetic resonance diffusion tensor imaging based fiber tracking is a unique approach that can reconstruct the three-dimensional pathways of white matter tracts based on voxel by voxel fiber orientation information *in vivo* [1]. Between the two common groups of fiber tracking algorithms[2-6], deterministic fiber tracking is more capable of providing affirmative and intuitionistic information[7-10] than probabilistic fiber tracking, and has been widely accepted in the fields of neurological evaluation and neurosurgical planning[11-13]. In particular, deterministic fiber tracking plays an important role in intraoperative visualization of white matter tracts to protect neurological function in an image-guided neuro-navigation system[14].

The neural fiber pathways that connect different regions of the brain exhibit the anatomical behaviors of smoothness and bending. The earlier deterministic fiber tracking algorithms usually adopted a single-tensor model to reconstruct fiber pathways, and the diffusion tensor field was built from raw multi-direction diffusion tensor imaging images[15-16]. The orientation of the tensor major eigenvector for each voxel is generally assumed to be parallel to local white matter fascicles[3]. Each individual fiber tract can be visualized by propagating a streamlined anterograde and retrograde direction from an initial seed point in the direction of the major eigenvector (tracking orientation) using a fixable spatial increment (step size). However, single-tensor deterministic fiber tracking does not display multiple fiber orientations for a complicated intra-voxel fiber configuration. More recently, novel multi-tensor models have been proposed to resolve this problem[17-19], and the geometrically constrained two-tensor model was developed into a deterministic algorithm of eXtended Streamline Tractography[20] in which only one orientation was chosen from the two directions at each planar voxel. With reliable tracking orientation, the two-tensor deterministic fiber tracking can accurately identify fiber bundles that were previously undetectable by conventional single-tensor fiber tracking at the regions of crossing fibers[20].

Despite the various deterministic fiber tracking methods, there are a number of limitations[3, 17-20], including the tracking orientation and the propagated step size. The tracking orientation provides the necessary direction information for any spatial point and ensures the possibility of passing through the regions of complex fiber configuration. Thus, the tracking direction remains of interest for development of planar voxels that possess complex fiber orientations. The size of the propagated step measures the distance moved along the tracking orientation at any point during the iteration of propagation. Clearly, the fixable step size cannot be used to faithfully represent fiber pathways at the subsections of abrupt bending fiber bundles, and would inevitably produce tracking errors.

The aim of this study was to develop a robust deterministic fiber tracking algorithm that solves the two aforementioned limitations. The method, termed the reliable tracking direction and flexible step size fiber tracking, is a new technique that provides robust tracking orientation and step size for propagation. For validation, we compare our method with the other two deterministic fiber tracking methods, single-tensor Fiber Assignment by Continuous Tracking and two-tensor eXtended Streamline Tractography, using synthetic phantom data and clinical human brain data.

RESULTS

Tracking results of branching and spiral phantom datasets with fixable and flexible step sizes

The tracking results of the branching and spiral datasets at the different step sizes are shown in Figure 1. Figures 1A–C show the tracking results of the branching phantom, and Figures 1D–F show the tracking results of the spiral phantom. At the top row of Figure 1, the three trackings start from a seed point, and only one fiber is reconstructed with the fixable step sizes (Figures 1A, B) and the flexible step size (Figure 1C). The upper parts of the three tracked branches are magnified two times and are placed at the right corner of Figures 1A–C. It is obvious that only the case of the flexible step could reach the extremity of the fibers and is superior to the other two cases using fixable step sizes. At the bottom row of Figure 1, it is evident that the tracking with the flexible step sizes (Figure 1F) could reach the farthest distance from the starting position compared with the other cases using fixable step sizes (Figures 1D, E). At the low curvature and high curvature situations, the fiber trackings with the flexible step size gave the better results.

Differences of tracking orientation using the single-tensor model and the two-tensor model

Figure 2 shows the original and the decomposed vectors of one central slice from the simulated fibers of the

orthogonal phantom data without noise. Figure 2A illustrates the principal eigenvector of the single tensor, where only one fiber tract direction could be shown in the intersected region labeled by the red rectangle. The two decomposed tracking orientations of the two-tensor model are shown in Figures 2B, C. After the decomposition, the horizontal directions of fiber tracts are displayed and have a similar direction to the horizontal configuration of the phantom data. The two decomposed vectors estimate the fiber pathways of the phantom data. It is obvious that the two-tensor model displayed more inherent orientation information than the single-tensor model. These data indicate that the planar voxels with two tracking orientations could be estimated using the two-tensor model.

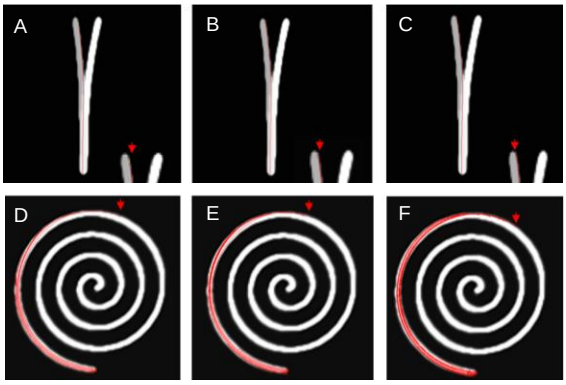

Figure 1 Comparison of tracking results with fixable and flexible step sizes.

(A–C) Tracking results of the branching dataset with fixable step sizes of two voxel units, one voxel unit, and flexible step size, respectively. (D–F) Tracking results of the spiral dataset with fixable step sizes of two voxel units, one voxel unit, and flexible step size, respectively. The red arrows represent the terminals of tracking, and the flexible trackings give better results than the fixable trackings.

Comparison of tracking efficiency using single-tensor Fiber Assignment by Continuous Tracking, two-tensor eXtended Streamline Tractography, and the proposed reliable tracking direction and flexible step size fiber tracking with phantom data

Figure 3 shows the tracking results of the phantom data using the three different methods. The tracking abilities were all weakened, with an increased level of noise from the left to the right and no fibers tracked for the dataset exhibiting a signal-to-noise ratio of 7:1. From the top row of Figure 3, it can be seen that one portion of the fiber tracts was not tracked by Fiber Assignment by Continuous Tracking. From the middle row of Figure 3, both the fiber tracts were partly tracked by eXtended Streamline Tractography. From the bottom row of Figure 3, it is clear that the simulated tracts were accurately tracked by our method. With a reliable tracking direction and step size, our method presents more detailed information than Fiber Assignment by Continuous Tracking and eXtended Streamline Tractography.

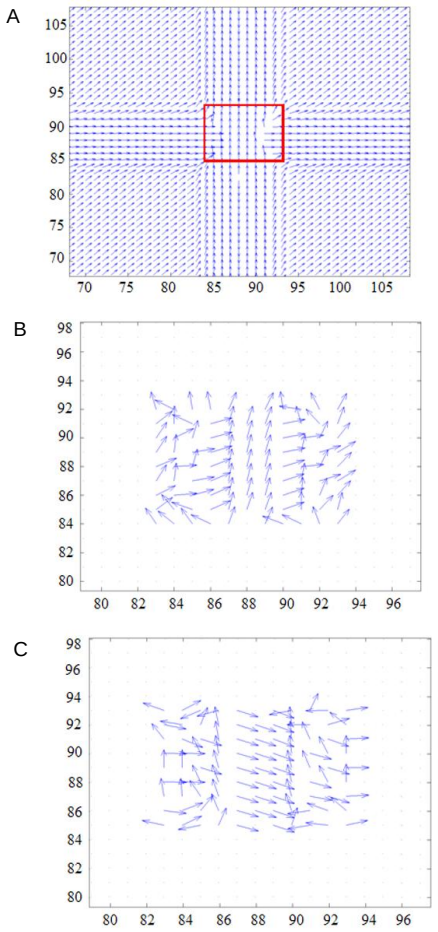

Figure 2 Comparison of the two tensor models using phantom data.

(A) Principal vectors from the single-tensor model.

(B) Vertical vectors from the two-tensor model.

(C) Horizontal vectors from the two-tensor model. The scales in the horizontal and vertical axes ranged from 68 to 108 with an increment of one pixel. The region denoted by the red rectangle is 10 × 10 pixels.

The tracking overlaid percentages of the three methods computed at four different signal-to-noise ratios are illustrated in Figure 4. It is apparent that our method had a higher tracking overlaid percentage than Fiber Assignment by Continuous Tracking and eXtended Streamline Tractography at the three high higher signal-to-noise ratios. With a further increase of noise, the tracking overlaid percentages of all the three methods decreased to zero as no fibers were tracked.

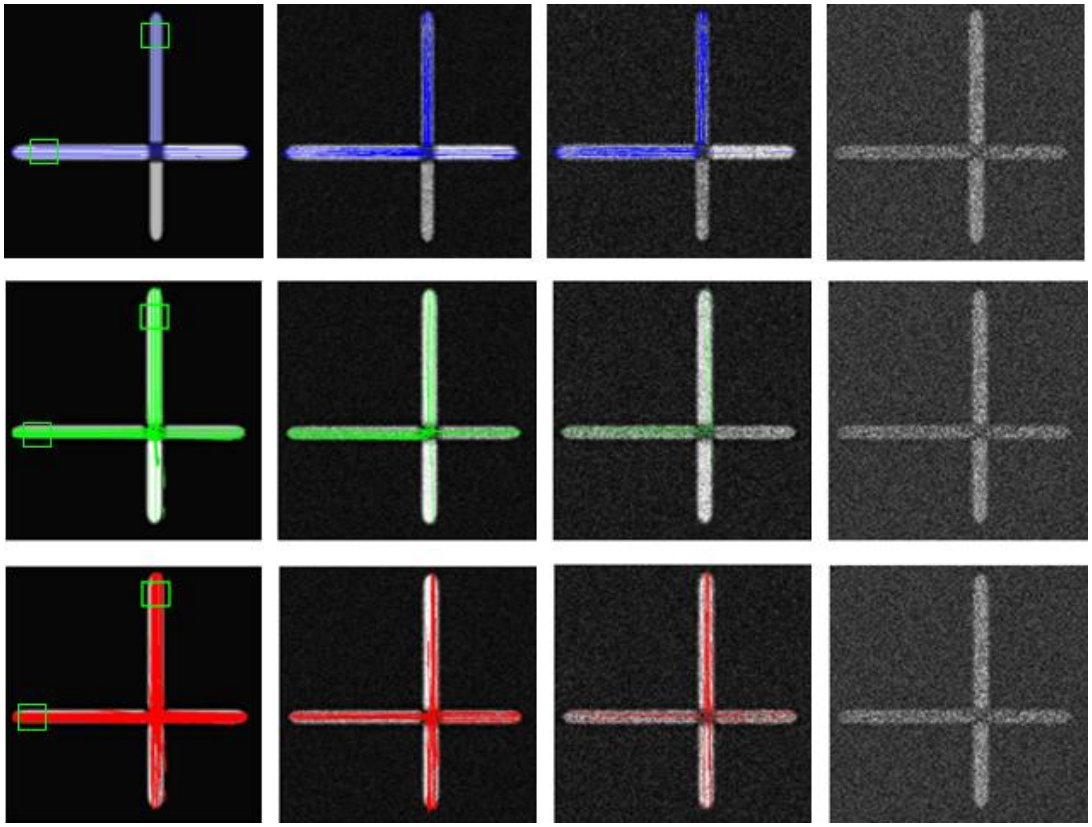

Figure 3 Comparison of tracking results with phantom datasets using three methods.

Top row: Results of Fiber Assignment by Continuous Tracking. Middle row: Results of eXtended Streamline Tractography. Bottom row: Results of proposed reliable tracking direction and the flexible step size fiber tracking. The columns from left to right indicate the results of data with different noise levels (without noise, signal-to-noise ratio 30:1, signal-to-noise ratio 15:1, and signal-to-noise ratio 7:1, respectively). Green rectangles denote the placement of regions of interest. The tracking of the proposed reliable tracking direction and the flexible step size fiber tracking produced the best match of fractional anisotropy image and tracked fibers.

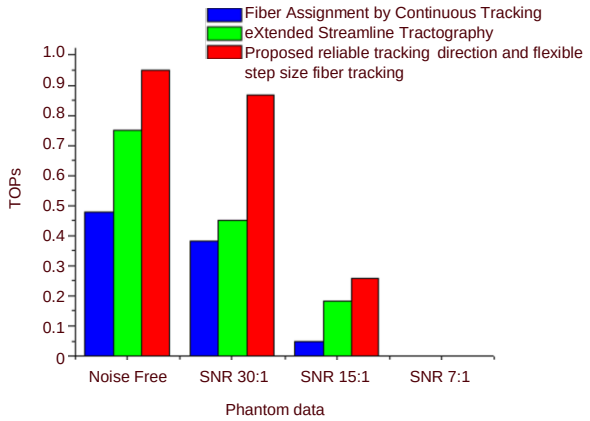

Figure 4 The tracking overlaid percentages (TOPs) of the three methods at four different levels of signal-to-noise ratio (SNR).

The TOP was computed by dividing $N_{tracking}$ with N_{true}. The TOP value was highest using proposed reliable tracking direction and the flexible step size fiber tracking, which indicates a superior capacity for restoration of original fiber configuration.

Comparison of tracking efficiency using single-tensor Fiber Assignment by Continuous Tracking, two-tensor eXtended Streamline Tractography, and the proposed reliable tracking direction and flexible step size fiber tracking with human data

Figure 5 shows the tracking results of the three fiber tracking methods for the healthy case. The tracked corpora callosa are overlaid with fractional anisotropy images using two different gray levels, and the three tracking results are shown in Figure 5. It is obvious that our method produced more detailed branches than for Fiber Assignment by Continuous Tracking and eXtended Streamline Tractography at the frontal forceps, splenium, and the body of the corpus callosum. Furthermore, the branches of the corpus callosum that extended into the occipital and frontal lobes are consistent with the white matter architecture in the fractional anisotropy images. Thus, our method is superior to Fiber Assignment by Continuous Tracking and eXtended Streamline Tractography for the reconstruction of corpus callosum pathways.

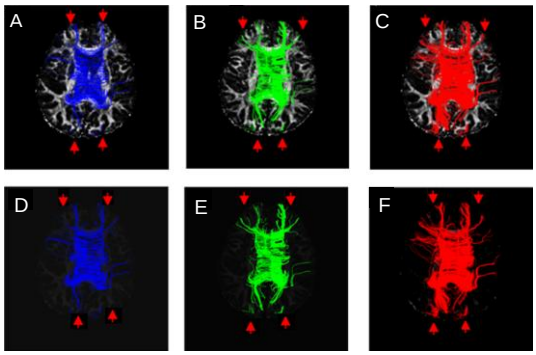

Figure 5 Comparison of tracking results for the healthy case (male, 42 years old).

(A) Corpus callosum tracked by Fiber Assignment by Continuous Tracking overlaid with fractional anisotropy image.

(B) Corpus callosum tracked by eXtended Streamline Tractography overlaid with fractional anisotropy image.

(C) Corpus callosum tracked by our method (proposed reliable tracking direction and the flexible step size fiber tracking) overlaid with fractional anisotropy image.

(D–F) Corpus callosum in (A–C) with different gray levels of fractional anisotropy image respectively.

The red arrows indicate that our method could detect fiber bundles more reliably than the other methods.

The tracking results of the case with low-grade glioma using the three fiber tracking methods are shown in Figure 6.

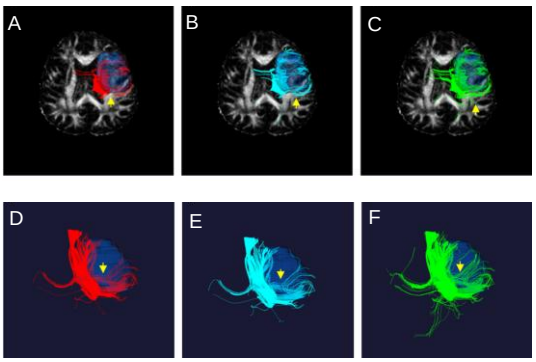

Figure 6 Comparison of tracking results for the low-grade glioma case (male, 45 years old; no medical therapy was delivered to the tumors prior to imaging) in axial and coronal views.

(A, D) Tracking results of Fiber Assignment by Continuous in red color.

(B, E) Tracking results of eXtended Streamline Tractography in indigo color.

(C, F) Tracking results of our method (proposed reliable tracking direction and the flexible step size fiber tracking) in green color.

The yellow arrows indicate the position of the main differences for the three tracking results. Our method displayed more detailed fiber bundles than the others methods in three-dimensional images.

The fractional anisotropy images, peritumoral fibers, and tumor mass are displayed in both axial and coronal views. The tumor mass is rendered using a blue color with a transparency value of 0.3. Compared with Fiber Assignment by Continuous Tracking and eXtended Streamline Tractography, our method revealed more completed peritumoral fibers. The differences between the three tracking methods are indicated by yellow arrows. The reconstructed fibers produced by our method were well matched with the imaging characteristics of the low-grade tumor. Our method reconstructed more detailed peritumoral fibers than Fiber Assignment by Continuous Tracking and eXtended Streamline Tractography, and the anatomical relationship between the tumor mass and peritumoral fibers could be precisely illustrated by our method.

DISCUSSION

In the present study, we developed a new fiber tracking method based on reliable tracking orientation and flexible step size. Compared with the Fiber Assignment by Continuous Tracking and eXtended Streamline Tractography methods, the proposed reliable tracking direction and flexible step size fiber tracking showed the best performance and could successfully track through regions with complicated fiber configurations. The two key innovative aspects of our study are: (1) we defined a new directional strategy based on the single-tensor model and the two-tensor model to select one optimal tracking orientation. This method provided a more reliable and optimal tracking orientation from each directional set. (2) A flexible step size was implemented in our method, which improved the accuracy of fiber tracking. For the evaluation of our proposed method, we used both phantom data and *in vivo* human data.

The flexible step size in our method was strongly associated with the curvature at every iterated step. The results of the phantom data show that the flexible step size was better than the fixable step size for the reconstruction of fiber configuration. This method can reduce the tracking errors by changing the scale, especially in the reconstruction of high curved fibers. As described above, the single-tensor model and the two-tensor model were used to simulate the orthogonal crossing of phantom data. It should be noted that the tensor model should represent the tracking orientation of fiber tracts. At the intersected region of the phantom data, the two tensor model produced both horizontal orientations and vertical orientations. However, the vertical orientations produced using the two-tensor model were different from the original

vertical orientation of the phantom data, which were accurately displayed by the single-tensor model. Thus, we kept the original direction in the directional set of planar voxels. These data suggest that our improved directional strategy may help the tracking to continue as far as possible at regions of complicated fiber architecture. To solve the nonlinear equations of the two-tensor model, the values of the four parameters were initiated by setting appropriate boundaries.

Our evaluation of the three fiber tracking methods using human data confirmed that our proposed method could faithfully reconstruct the fiber tracts consistent with the architecture of nerve fibers. For the low-grade glioma, it is generally considered that the tumor mass does not infiltrate or invade surrounding neural fibers. The peritumoral fibers reconstructed by our method conformed to the imaging characteristics of a benign tumor. Since the anatomical relationship of the tumor mass and peritumoral fibers is important to determine clinically, our method may be helpful for preoperative tumor grading[21], surgical planning, and intra-operative guidance[22].

There were two limitations to our study. First, no denoising strategy was used in our approach. The results of our phantom data indicate that a higher noise level deteriorates the performance of our method, as the noise shifts eigenvectors and increases eigenvalues[23]. Development of a denoising strategy for our method will form part of future studies. Second, the evaluation of our method using human data requires improvement. In our experiment, we were unable to perform quantitative evaluation of fiber tracking on *in vivo* data, as required for a gold standard[24]. Therefore, the use of *in vitro* organ models may be another aspect of our future work.

In conclusion, our approach was superior to Fiber Assignment by Continuous Tracking and eXtended Streamline Tractography for showing the details of fiber bundles, which were in good agreement with known anatomy.

MATERIALS AND METHODS

Design

Neuroimaging, algorithm research.

Time and setting

This study was conducted at the Digital Medical Research Center, Shanghai Medical School, Fudan University, China from July 2010 to March 2012.

Materials

Phantom data

We used Phantom Images for Simulating Tractography Errors[25] data to evaluate the performance of our method. The Phantom Images for Simulating Tractography Errors data sets contain numerous different simulated fiber tracts. The tracts were generated by simulating a diffusion tensor imaging measurement with 30 diffusion weighted images and four unweighted images using the following parameters: number of diffusion encoding directions = 30, *b* value = 1 000 s/mm^2, echo time = 90 ms, number of excitations = 4, image resolution = 1 × 1 × 1 mm^3, image size = 150 × 150 × 16. There were 10 different trajectory structures in total, each possessing four data sets with different signal-to-noise ratio levels (without noise, 7:1, 15:1, and 30:1). The simulated tracts were overlaid on isotropic, homogeneous backgrounds in diffusion weighted imaging images. In our experiments, only the trajectories of branching, spiral, and orthogonal crossings were used.

Human data

We also used human data to assess the performance of our method. Two sets, one from a healthy volunteer and the other from a patient with low-grade glioma[26], of diffusion tensor imaging images were kindly provided by the Department of Neurosurgery of Huashan Hospital, Fudan University in China. The diffusion tensor imaging datasets were acquired using a 3 T MRI scanner (Sigma Excite, GE Medical Systems, Bethesda, MD, USA) with a multi-slice single shot spin echo diffusion weighted echo planar imaging sequence (echo time = 70–90 ms, repetition time = 7 000–8 000 ms, slice thickness = 5–7 mm, thick gap = 1 mm, matrix size = 128 × 128, field of view = 24 × 24 cm^2, *b* = 1 000 s/mm^2, 15 non-collinear gradient directions). A GE birdcage head coil was used for the two cases. The corresponding T1-weighted imaging (T1WI) or T2WI was acquired with a spin echo sequence (field of view = 24 × 24 cm^2, repetition time = 2 000–2 280 ms, echo time = 18–20 ms, slice thickness = 7–10 mm, thick gap = 1 mm). This study was carried out according to the standard procedures of the Hospital Ethics Committee and with the consent of the two human subjects. Entry criteria for this study were: (A) a healthy adult volunteer and with normal intelligence, and (B) one patient with a low-grade glioma who received no medical therapy for the tumors prior to imaging.

Methods

Research way

The tracking orientation and the step size are vital in any deterministic fiber tracking algorithm. In our method, a

defined directional strategy was used to select one optimal tracking orientation from one directional set built from a single-tensor model[14] and a two-tensor model[19]. A flexible step size was also applied, which allows the propagation to continue as soon as possible, and the terminal criteria were evaluated at every step of propagation.

Overview of the reliable tracking direction and flexible step size fiber tracking algorithm

The tracking of fibers is a successive process that follows only one orientation at any point, and is regulated by many pre-defined terminal criteria such as fractional anisotropy values, deflection angle, and image boundary. For every seed point *P*, the propagation was defined as:

$$P_{n+1}=P_n+SV_{Pn} \quad (n = 0, 1, 2 \ldots) \quad (1),$$

where P_n is the initial point; V_{Pn}, the direction of point P_n, *S*, the unit of propagated step, and P_{n+1}, the next point of the propagated pathway at the direction V_{Pn} through the length of propagated step *S*.

Single-tensor model and two-tensor model

In a diffusion-weighted MRI experiment, multi-direction gradient pulses are induced, and the amount of signal loss *S* when compared with the original signal S_0 (without diffusion weighting) was modeled by the following equation[14]:

$$S = S_0 e^{-bg^t D\ \mathrm{g}} \quad (2).$$

Here, *S* stands for the diffusion weighted signal; S_0, the signal without any diffusion weighted gradients; *g*, a unit vector representing the direction of a diffusion gradient; g^t, a transposed form of *g*; *b*, a factor describing the gradient timing and strength; and *D*, the estimated tensor for every voxel. Every diffusion tensor *D* is geometrically equivalent to an ellipsoid, with the three eigenvectors of the diffusion tensor *D* as the radii of the diffusion ellipsoid and their associated eigenvalues as the hemiaxis lengths. The shapes of the ellipsoids for voxels are classified as linear anisotropic diffusion, planar anisotropic diffusion, or isotropic diffusion[27].

The two-tensor model proposed by Peled *et al* [19] was used to fit one single tensor *D* into the two tensors D_a and D_b at each planar voxel. The planar voxels were selected by the index of planar anisotropy, C_P, which is the Westin's planar index[28]. The two-tensor model assumes that two fiber tracts are constrained in the plane spanned by the first two principal eigenvectors ($\hat{e}_1, \hat{e}_2$) of single tensor *D*. The signal attenuation equation for the constrained two-tensor model can be described by a weighted sum of two Gaussian functions:

$$S = S_0(fe^{-bg_T{}^t D_a g_T} + (1-f)e^{-bg_T{}^t D_b g_T}) \quad (3).$$

Here, *S* stands for the diffusion weighted signal; S_0, the signal without any diffusion weighted gradients; *f*, the fraction of the first tensor; g_T, a unit vector representing a transformed diffusion gradient *g*; $g_T{}^t$, a transposed form of g_T; *b*, a factor describing the gradient timing and strength; and D_a and D_b, the decomposed tensors at one planar voxel, and are formulated as follows:

$$D_a = \begin{bmatrix} d_{a1} & d_{a3} & 0 \\ d_{a3} & d_{a1} & 0 \\ 0 & 0 & \lambda_3 \end{bmatrix} \quad D_b = \begin{bmatrix} d_{b1} & d_{b3} & 0 \\ d_{b3} & d_{b1} & 0 \\ 0 & 0 & \lambda_3 \end{bmatrix} \quad (4),$$

where:

$$\begin{aligned} d_{p1} &= \cos^2\phi_p\lambda_1 + \sin^2\phi_p\lambda_3, p \in \{a,b\} \\ d_{p2} &= \sin^2\phi_p\lambda_1 + \cos^2\phi_p\lambda_3 \\ d_{p3} &= \cos\phi_p \sin\phi_p(\lambda_1 - \lambda_3) \end{aligned} \quad (5).$$

Here, λ_1 stands for the principal eigenvalue that is assumed to be the same for both of the fiber tracts; ϕ_a and ϕ_b, the angles subtended by the principal diffusion directions in the plane; and λ_3, calculated from the single-tensor fit.

In actual computation, the vectors of the diffusion gradients *g* should be transformed into g_T in the new coordinate system defined by the three eigenvectors of each single-tensor fit at the planar voxel, and the rotation matrix *R* is defined as follows:

$$R = \begin{bmatrix} u_{x1} & u_{y1} & u_{z1} & 0 \\ u_{x2} & u_{y2} & u_{z2} & 0 \\ u_{x3} & u_{y3} & u_{z3} & 0 \\ 0 & 0 & 0 & 1 \end{bmatrix} \quad (6),$$

where (u_{x1}, u_{y1}, u_{z1}), (u_{x2}, u_{y2}, u_{z2}), and (u_{x3}, u_{y3}, u_{z3}) are the first, the second, and the third eigenvectors, respectively, of the single tensor *D*.

Equation (3) can be solved using a nonlinear least-squares method with boundary constraints, based on the interior-reflective Newton method[29], which was implemented in Matlab software (Mathworks, Natick, MA, USA).

Directional strategy

The defined directional strategy was used to select one appropriate tracking orientation from every directional set. The directional set of linear voxel contains only one principal vector of the single-tensor *D*. For every planar voxel, the single tensor *D* is fitted into two tensors, D_a and D_b, and produces two new principal vectors. These two new vectors, together with the principal vector of the original single tensor *D*, form a directional set from which the tracking orientation is selected. The tracking orientation was chosen strategically by minimizing the deflection angle between the vectors at the current and previous points.

The directional strategy is expressed as follows:
At one point within linear voxel,

$$v_p = \begin{cases} v_t & if\ \cos\langle v_t \cdot v_i \rangle > \theta_{threshod},\ v_t = v_s \\ -v_t & if\ \cos\langle v_t \cdot v_i \rangle > -\theta_{threshod}, v_t = v_s \end{cases} \quad (7),$$

or one point within planar voxel,

$$v_p = \begin{cases} v_t & if\ \min\{\cos\langle v_t \cdot v_i \rangle : \cos\langle v_t \cdot v_i \rangle > \theta_{threshod},\ v_t \in \{v_s, v_a, v_b\}\} \\ -v_t & if\ \min\{\cos\langle v_t \cdot v_i \rangle : \cos\langle v_t \cdot v_i \rangle > -\theta_{threshod}, v_t \in \{v_s, v_a, v_b\}\} \end{cases} \quad (8).$$

Here, v_s stands for the principal vector from single tensor *D* for each voxel; v_a and v_b, the two decomposed principal vectors from two tensors D_a and D_b; v_i, the vector of the last point; and $\theta_{threshold}$, the deflection angle computed by the vectors v_t and v_i. If the value of $\theta_{threshold}$ is positive, v_t does not change, while if the value of $\theta_{threshold}$ is negative, v_t should change into the opposite direction.

Flexible propagated step size

In our algorithm, the flexible step size was implemented and changed along with the deflection angle between the current point and the last point. The flexible step size *S* is defined as follows:

$$S = \frac{1}{2 * \max\{|V_{Pn}(0)|, |V_{Pn}(1)|, |V_{Pn}(2)|\}} * |(\cos\langle v_t \cdot v_i \rangle)| \quad (9).$$

Here, $V_{pn}(0)$, $V_{pn}(1)$, and $V_{pn}(2)$ represent the first, second, and third element of the vector at a given point *n*. $|(\cos)\langle v_t \cdot v_i \rangle|$ is the absolute value of the deflection angle computed by the vectors v_t and v_i as mentioned above.

This scheme is more effective than the fixable step size in displaying curved fiber pathways (Figure 7). The same intervals separated by the blue dashed lines have the same tracking orientation. Compared with the neural fiber pathway (black curve), the tracked pathway in the green point line more accurately reflects the fiber representation than that in the red point line.

The setup of fiber tracking method

The main steps of our fiber tracking are as follows:
(1) Build the tensor field using the single-tensor model from multi-directional diffusion tensor imaging raw images.
(2) Compute the eigenvectors and eigenvalues of every tensor.
(3) Choose one region of interest or two regions of interest *via* manual delineation.
(4) Find and decompose planer voxels. The threshold of C_p decides the number of planar voxels needed to be decomposed. The larger the threshold, the less planar voxels are fitted by the two-tensor model. The directional sets of planar and linear voxels are formed.
(5) Start tracking from the seed points in the region of interest. The seed points are interpolated for every voxel with a ratio of 3:1. In turn, tracking initiates from its two decomposed directions at every planar voxel in the region of interest, and start from only one direction at every linear voxel in the region of interest. The defined directional strategy is used to select one tracking orientation from the directional set. The parameters of terminal criteria are chosen by prior experience.
(6) The tracked points are reorganized into streamlines with two parameters of fibers number and point number for each fiber.

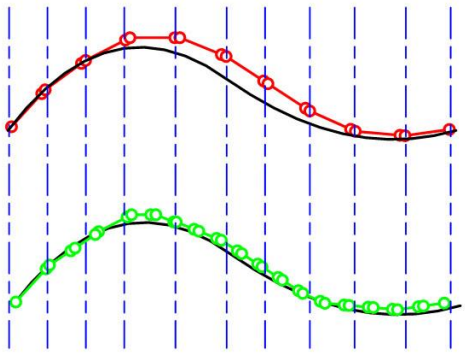

Figure 7 Comparison of tracking efficiency using fixable and flexible step sizes.

The neural fiber pathway is represented by the black curve, and the red point line and green point line show the tracked routes in fixable and flexible step sizes, respectively.

Experiments

The phantom data and the human data were both

tracked by the Fiber Assignment by Continuous Tracking, the eXtended Streamline Tractography, and our method, and comparisons between made qualitatively by three experienced radiologists. For the phantom data, the tests of flexible step size, tracking orientation, and tracking performance were performed. Furthermore, the phantom data were quantitatively evaluated by computing the index of tracking overlaid percentage.

Test of flexible step size with phantom data

For evaluating the effect of step size in fiber tracking, the two datasets of branching and spiral without noise were used. The two simulated datasets are considered to have lots of linear voxels and no planar voxels, thus the single-tensor Fiber Assignment by Continuous Tracking was applied for the test. The branching dataset has low curvature, and the single-tensor Fiber Assignment by Continuous Tracking with fixable step sizes or flexible step size is compared. The curvature of spiral dataset is high and the same experiments are performed. For clear observation, the tracking results are overlaid with the fractional anisotropy images.

Test of tracking orientation with phantom data

The single-tensor model and two-tensor model were evaluated by the dataset of orthogonal crossing without noise. At the intersecting region, there are many planar voxels containing two directions of fiber tracts. The single-tensor model and two-tensor model are used to simulate the fiber pathways. The accuracy of the simulation reflects the capacity of two tensor models in restoring the configuration of the fiber tracts.

Test of tracking performance with phantom data

The datasets of orthogonal crossing were used to compare the performance of the three different fiber tracking methods. The intersected region of the phantom data is modeled as having a complex fiber configuration. The main parameters for fiber tracking on the phantom dataset were as follows: the fiber tracking threshold was 0.1; the threshold of the turning angle was 0.95 rad; the threshold of the background was 30 for the phantom without noise and 80 for the phantoms with noise; the maximum fiber length used 400 iterations; and the minimum length used 80 iterations. The hand-drawn region of interest was located on both sections of the simulated tracts. The planar index of C_p was selected as 0.25. In addition, we calculated the index of tracking overlaid percentage to quantitatively compare the results of tracking. A larger index of tracking overlaid percentage indicates that more voxels of phantom data are tracked by the tested algorithm. Let $N_{tracking}$ is the number of voxels tracked by the tested algorithm, and N_{true} is the number of voxels containing simulated fiber bundles. The tracking overlaid percentage is computed by dividing $N_{tracking}$ with N_{true}, as follows:

$$TOP = \frac{N_{tracking}}{N_{true}} \quad (10)$$

Human data experiments

The three different fiber tracking methods were also compared using the two human datasets. Since the corpus callosum is the largest white matter structure in human brain and carries the majority of communication between the two brain hemispheres, the corpus callosum of the healthy case was used to evaluate the three fiber tracking methods. Each tracked corpus callosum was overlaid with the fractional anisotropy images to determine whether the tracked corpus callosum could reach the lobes of brain. For the case with low-grade glioma, the peritumoral fibers surrounding the tumor mass were tracked. The low-grade glioma was closely enclosed by adjacent fibers without infiltration or erosion. For both cases, the regions of interest were delineated by the radiologists, and the main tracking parameters were chosen as follows: the fractional anisotropy threshold was set to 0.15, the threshold of the turning angle was 0.90 rad, and the planar index of C_p was 0.30.

Funding: This work was partly supported by the Science and Technology Commission of the Shanghai Municipality of China, No. 10dz2211800, No.10XD1421400; the National High Technology Research and Development Program, No. 2009AA02Z415; and the Innovation Program of Shanghai Municipal Education Commission, No. 11yz292.

Author contributions: Xufeng Yao was responsible for study design, collected data, and performed the phantom data and human data experiments. Xufeng Yao and Zhijian Song evaluated the experiment results. Xufeng Yao, Manning Wang, Xinrong Chen, Zhexu Li, Xiaoping Xu, Xuelong Zhang, and Shengdong Nie were in charge of manuscript writing. All authors approved the final version of the paper.

Conflicts of interest: None.

Ethical approval: This study received permission from the Ethics Committee of Fudan University in China.

Author statements: The manuscript is original, has not been submitted to or is not under consideration by another publication, has not been previously published in any language or any form, including electronic, and contains no disclosure of confidential information or authorship/patent application/funding source disputations.

REFERENCES

[1] Vargas MI, Viallon M, Nguyen D, et al. Diffusion tensor imaging (DTI) and tractography of the brachial plexus: feasibility and initial experience in neoplastic conditions. Neuroradiology. 2010;52(3):237-245.

[2] Mori S, van Zijl PC. Fiber tracking: principles and strategies-a technical review. NMR Biomed. 2002;15(7-8):468-480.

[3] Jiang H, van Zijl PC, Kim J, et al. DtiStudio: resource program for diffusion tensor computation and fiber bundle tracking. Comput Methods Programs Biomed. 2006;81(2): 106-116.

[4] Behrens TE, Woolrich MW, Jenkinson M, et al. Characterization and propagation of uncertainty in diffusion-weighted MR imaging. Magn Reson Med. 2003;50(5):1077-1088.

[5] Behrens TE, Berg HJ, Jbabdi S, et al. Probabilistic diffusion tractography with multiple fibre orientations: What can we gain? Neuroimage. 2007;34(1):144-155.

[6] Zhang F, Hancock ER, Goodlett C, et al. Probabilistic white matter fiber tracking using particle filtering and von Mises-Fisher sampling. Med Image Anal. 2009;13(1):5-18.

[7] Nimsky C, Ganslandt O, Hastreiter P, et al. Preoperative and intraoperative diffusion tensor imaging-based fiber tracking in glioma surgery. Neurosurgery. 2005;56(1): 130-137.

[8] Setzer M, Murtagh RD, Murtagh FR, et al. Diffusion tensor imaging tractography in patients with intramedullary tumors: comparison with intraoperative findings and value for prediction of tumor resectability. J Neurosurg Spine. 2010;13(3):371-380.

[9] Wang YX, Zhu XL, Deng M, et al. The use of diffusion tensor tractography to measure the distance between the anterior tip of the Meyer loop and the temporal pole in a cohort from Southern China. J Neurosurg. 2010;113(6): 1144-1151.

[10] Buchmann N, Gempt J, Stoffel M, et al. Utility of diffusion tensor-imaged (DTI) motor fiber tracking for the resection of intracranial tumors near the corticospinal tract. Acta Neurochir (Wien). 2011;153(1):68-74.

[11] Tatsuzawa K, Owada K, Sasajima H, et al. Surgical strategy of brain tumors adjacent to the optic radiation using diffusion tensor imaging-based tractography. Oncol Lett. 2010;1(6):1005-1009.

[12] Spena G, Nava A, Cassini F, et al. Preoperative and intraoperative brain mapping for the resection of eloquent-area tumors. A prospective analysis of methodology, correlation, and usefulness based on clinical outcomes. Acta Neurochir (Wien). 2010;152(11): 1835-1846.

[13] Qiu TM, Zhang Y, Wu JS, et al. Virtual reality presurgical planning for cerebral gliomas adjacent to motor pathways in an integrated 3-D stereoscopic visualization of structural MRI and DTI tractography. Acta Neurochir (Wien). 2010;152(11):1847-1857.

[14] Basser PJ, Pajevic S, Pierpaoli C, et al. In vivo fiber tractography using DT-MRI data. Magn Reson Med. 2000;44(4):625-632.

[15] Masutani Y, Aoki S, Abe O, et al. MR diffusion tensor imaging: recent advance and new techniques for diffusion tensor visualization. Eur J Radiol. 2003;46(1):53-66.

[16] Lenglet C, Campbell JS, Descoteaux M, et al. Mathematical methods for diffusion MRI processing. Neuroimage. 2009;45(1 Suppl):S111-122.

[17] Kreher BW, Schneider JF, Mader I, et al. Multitensor approach for analysis and tracking of complex fiber configurations. Magn Reson Med. 2005;54(5):1216-1225.

[18] Pasternak O, Assaf Y, Intrator N, et al. Variational multiple-tensor fitting of fiber-ambiguous diffusion-weighted magnetic resonance imaging voxels. Magn Reson Imaging. 2008;26(8):1133-1144.

[19] Peled S, Friman O, Jolesz F, et al. Geometrically constrained two-tensor model for crossing tracts in DWI. Magn Reson Imaging. 2006;24(9):1263-1270.

[20] Qazi AA, Radmanesh A, O'Donnell L, et al. Resolving crossings in the corticospinal tract by two-tensor streamline tractography: Method and clinical assessment using fMRI. Neuroimage. 2009;47 Suppl 2:T98-106.

[21] Nilsson D, Rutka JT, Snead OC, et al. Preserved structural integrity of white matter adjacent to low-grade tumors. Childs Nerv Syst. 2008;24(3):313-320.

[22] Pamir MN, Ozduman K, Dinçer A, et al. First intraoperative, shared-resource, ultrahigh-field 3-Tesla magnetic resonance imaging system and its application in low-grade glioma resection. J Neurosurg. 2010;112(1): 57-69.

[23] Laun FB, Schad LR, Klein J, et al. How background noise shifts eigenvectors and increases eigenvalues in DTI. MAGMA. 2009;22(3):151-158.

[24] Lu Y, Aldroubi A, Gore JC, et al. Improved fiber tractography with Bayesian tensor regularization. Neuroimage. 2006;31(3):1061-1074.

[25] Deoni S. Phantom Images for Simulating Tractography Errors. 2005. http://cubric.psych.cf.ac.uk/commondti.

[26] Kleihues P, Cavence WK. World Health Organization Classification of Tumours Pathology and Genetics Tumours of the Nervous System. Lyon: IARCPres. 2000.

[27] Alexander AL, Hasan K, Kindlmann G, et al. A geometric analysis of diffusion tensor measurements of the human brain. Magn Reson Med. 2000;44(2):283-291.

[28] Westin CF, Maier SE, Mamata H, et al. Processing and visualization for diffusion tensor MRI. Med Image Anal. 2002;6(2):93-108.

[29] Coleman TF, Li Y. A reflective newton method for minimizing a quadratic function subject to bounds on some of the variables. Siam J Optimiz. 1996;6(4): 1040-1058.

(Reviewed by Dean J, Rave W, Chen F, Yang JP)
(Edited by Wang LM, Qiu Y, Li CH, Song LP)